

Journal of Materials Chemistry B

Materials for biology and medicine

Accepted Manuscript

This article can be cited before page numbers have been issued, to do this please use: L. JIQIANG, A. Z. Abdulkadir, S. Wu, Y. Gao, B. J. Butuyuyu, K. M. Wong, C. Lee, L. Cai, J. Chen and P. Zhang, *J. Mater. Chem. B*, 2025, DOI: 10.1039/D5TB00758E.



This is an Accepted Manuscript, which has been through the Royal Society of Chemistry peer review process and has been accepted for publication.

Accepted Manuscripts are published online shortly after acceptance, before technical editing, formatting and proof reading. Using this free service, authors can make their results available to the community, in citable form, before we publish the edited article. We will replace this Accepted Manuscript with the edited and formatted Advance Article as soon as it is available.

You can find more information about Accepted Manuscripts in the [Information for Authors](#).

Please note that technical editing may introduce minor changes to the text and/or graphics, which may alter content. The journal's standard [Terms & Conditions](#) and the [Ethical guidelines](#) still apply. In no event shall the Royal Society of Chemistry be held responsible for any errors or omissions in this Accepted Manuscript or any consequences arising from the use of any information it contains.

ARTICLE

Cyanine-scaffold Fluorogenic Probes for Visual Detection of Nitroreductase in Living Bacteria

Jiqiang Liu^{a,c,e}, Abdulkadir Zakari Abdulkadir^{a,b}, Siye Wu^c, Yonghui Gao^d, Baraka Joseph Butuyuyu^{a,b}, Keith Man-Chung Wong^c, Chi-Sing Lee^e, Lintao Cai^a, Jihong Chen^d, Pengfei Zhang^{*a}

Received 00th January 20

Accepted 00th January 20xx

DOI: 10.1039/x0xx00000x

Bacterial infections pose significant challenges in clinical diagnostics and microbiological research due to the need for rapid, sensitive, and specific detection methods. Herein, we report the development of **Cy5-NO₂**, a novel nitro-containing fluorescent probe designed for real-time monitoring of bacterial nitroreductase (NTR) activity. **Cy5-NO₂** is synthesized through a streamlined, high-yield process without chromatography, yielding a stable compound confirmed by X-ray crystallography and spectroscopic methods. The probe exhibits negligible fluorescence in its native state but undergoes a 30-fold fluorescence enhancement at 620 nm upon NTR-mediated reduction of the nitro group to an amino group, with a detection limit of 10 ng/mL. Time-dependent density functional theory (TDDFT) calculations reveal that the fluorescence "turn-on" mechanism arises from a transition from charge-transfer quenching (in **Cy5-NO₂**) to local excitation (in **Cy5-NH₂**), as supported by a significant increase in oscillator strength. The probe demonstrates high specificity for NTR under physiological conditions and successfully detects live bacterial cells (e.g., *E. coli* and *S. aureus*) via confocal laser scanning microscopy (CLSM). The combination of direct nitro-to-amine reduction, exceptional stability, and minimal enzymatic interference positions **Cy5-NO₂** as a promising tool for universal bacterial detection, advancing applications in clinical diagnostics and microbial imaging.

Introduction

Bacteria play pivotal roles in various biological processes, ranging from beneficial interactions within the human microbiome to causing severe diseases. Detecting pathogenic bacteria is crucial for diagnosing infections and guiding appropriate therapeutic interventions.¹⁻⁴ Pathogenic strains such as *Escherichia coli*, *Staphylococcus aureus*, *Klebsiella pneumoniae*, *Acinetobacter baumannii*, and *Pseudomonas aeruginosa* are responsible for significant morbidity and mortality worldwide.⁵⁻⁷ Accurate identification of these pathogens is essential not only for effective treatment but also for monitoring antibiotic resistance patterns.⁸⁻⁹ While traditional methods such as culture-based techniques¹⁰, nucleic acid amplification¹¹, and mass spectrometry¹² are reliable, they

are often time-consuming and resource-intensive. Therefore, there is an urgent need for innovative approaches that can quickly, sensitively, and accurately identify bacterial pathogens. Fluorescence imaging has emerged as a powerful tool for bacterial detection due to its high sensitivity, real-time capability, and spatial resolution.¹³⁻¹⁸ Among fluorescence-based strategies, fluorescent probes targeting nitroreductase (NTR), an enzyme highly conserved among bacteria,^{19,20} offer a promising avenue for universal bacterial detection.^{21,22} NTR catalyzes the reduction of nitroaromatic compounds using nicotinamide adenine dinucleotide (phosphate) (NAD(P)H) as a cofactor, making it an ideal target for developing "turn-on" fluorescence probes. These probes remain non-fluorescent until they encounter active NTR, at which point they emit a strong signal, enabling precise localization and quantification of bacterial presence. The advantage of this "turn-on" mode lies in its ability to significantly reduce background noise caused by autofluorescence or non-specific interactions, thereby enhancing detection accuracy.²³⁻²⁴ However, existing NTR-targeted fluorescent probes often suffer from limitations such as complex synthesis routes, short emission wavelengths, poor stability and insufficient sensitivity or selectivity.²⁵⁻²⁷ Addressing these issues requires the development of new probes that are simpler to synthesize, exhibit longer emission wavelengths, stable in biological media and demonstrate enhanced performance.

In this study, we introduce **Cy5-NO₂**, a novel nitro-containing fluorescent probe designed for the real-time monitoring of

^a Guangdong Key Laboratory of Nanomedicine, CAS-HK Joint Lab of Biomaterials, CAS Key Laboratory of Biomedical Imaging Science and System, Shenzhen Engineering Laboratory of Nanomedicine and Nanoformulations, CAS Key Lab for Health Informatics, Shenzhen Institutes of Advanced Technology, Chinese Academy of Sciences, Shenzhen, 518055, China. E-mail: pf.zhang@siat.ac.cn

^b University of Chinese Academy of Sciences, Beijing, 100049, China

^c Department of Chemistry, Southern University of Science and Technology, Shenzhen, 518055, China

^d Department of Healthcare-associated Infection Control, People's Hospital of Bao'an District, Shenzhen, Shenzhen, 518101, China

^e Department of Chemistry, Hong Kong Baptist University, Kowloon Tong, Hong Kong SAR, China

[†] J. Q. Liu and A.Z. Abdulkadir contributed equally to this work.

Supplementary Information available: [details of any supplementary information available should be included here]. See DOI: 10.1039/x0xx00000x



ARTICLE

Journal Name

bacterial NTR activity. Synthesized through a straightforward and efficient process, **Cy5-NO₂** exhibits remarkable stability and specificity toward NTR. Upon reduction by NTR, the probe displays a 30-fold increase in fluorescence intensity at 620 nm, with a detection limit of 10 ng/mL. Unlike previously reported self-immolative cleavage-type cyanine-based probes such as the heptamethine systems (Smith et al.), which require multi-step modifications to achieve nitroreductase responsiveness, leading to increased production costs and poor stability due to inherent polyene linkers of heptamethine structure and hydrolyzable functional groups²⁸, or "turn-off" probes like **Cy7-NO₂** (Sui et al.) which necessitate signal inversion for clinical interpretation²⁹, **Cy5-NO₂** operates via direct nitro-to-amine reduction. This streamlined mechanism eliminates auxiliary functional groups, thereby avoiding interference from hydrolytic enzymes (e.g., esterases/proteases) inherent to prior systems. Emitting at 620 nm, **Cy5-NO₂** achieves a balance between reduced autofluorescence and compatibility with standard confocal microscopy setups, enabling robust real-time imaging of live bacteria, as demonstrated by its successful application in detecting *E. coli* and *S. aureus* via Confocal Laser Scanning Microscope. Furthermore, its minimalist design enhances stability, while column-free synthesis and cost-efficient production underscore scalability for industrial translation. These findings highlight the potential of **Cy5-NO₂** as a valuable tool for sensitive and specific bacterial detection and imaging, advancing microbiological research and clinical diagnostics. By overcoming the limitations of current probes, **Cy5-NO₂** represents a significant advancement in bacterial detection, offering enhanced sensitivity and specificity that pave the way for more effective diagnostic tools and therapeutic strategies against bacterial infections.

Results and discussion

Design and synthesis of probe Cy5-NO₂

Nitroaromatic compounds can serve as biomarkers for the detection of bacterial nitroreductases (NTRs), as they are enzymatically reduced to nitrile, hydroxylamine, and amino derivatives by NADH/NADPH cofactors.³⁰ The synthetic pathway for **Cy5-NO₂** is outlined in Fig. 1A. The synthesis began with **Cy5-Cl**, a near-infrared (NIR) luminescent reporter, which was reacted with acetylacetone in the presence of Et₃N as a catalyst to afford **Cy5-acac**. Subsequently, **Cy5-acac** underwent a heterocyclization reaction with p-nitroaniline, the NTR-responsive moiety, yielding the target probe, **Cy5-NO₂**. Notably, this final step is highly efficient, characterized by the precipitation of a blue-violet solid, which can be purified via simple filtration without requiring column chromatography, resulting in a reaction yield of 92%. This streamlined process ensures high reproducibility and cost-effectiveness, addressing a critical bottleneck in cyanine dye manufacturing. Blue crystals suitable for structural analysis were obtained by a diffusion system of diethyl ether and acetonitrile solution. The structure

of **Cy5-NO₂** was fully characterized using ¹H NMR, ¹³C NMR, and high-resolution mass spectrometry (HR-MS) (See supporting information), providing conclusive evidence for its identity. The molecular structure of **Cy5-NO₂** has been detected by X-ray crystallography (XRD). The perspective drawing of **Cy5-NO₂** is presented in Fig. S1. The supplementary crystallographic data for **Cy5-NO₂** are summarized in Table S1, and the selected bond lengths (in Å) and bond angles (in degrees) of **Cy5-NO₂** are listed in Table S2. The benzindole unit and the middle heterocyclic core in **Cy5-NO₂** structure are nearly planar (Fig. S1). A distortion angle of 76.5° is observed between the central heterocyclic ring (C14-C15-N2-C22-C23-C24) and the p-nitrobenzene ring (C16-C17-C18-C19-C20-C21). This angular displacement alleviates the steric hindrance between these two rings, contributing to enhanced molecular stability. Additionally, the absence of hydrolysable moieties ensures resistance to enzymatic degradation, a critical feature for in vivo applications.

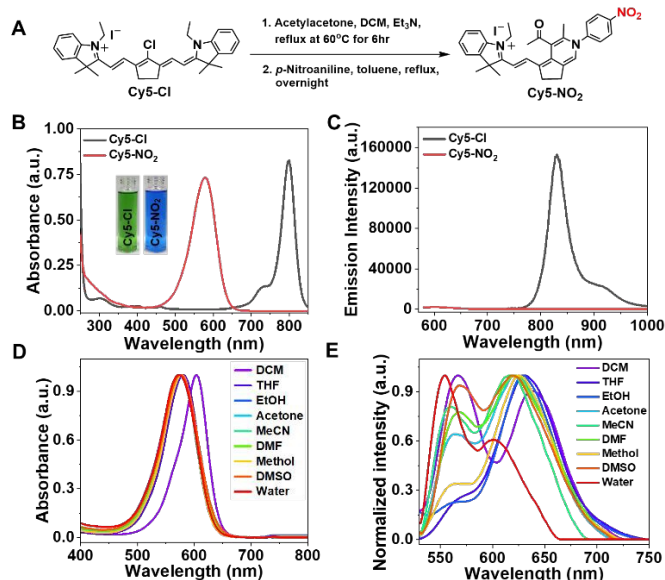


Fig. 1 (A) Synthetic route of **Cy5-NO₂** (probe). (B) Absorption and (C) emission spectra of **Cy5-Cl** and **Cy5-NO₂** in PBS buffer (10 mM, pH 7.4, 10% DMSO). Normalized absorption (D) and emission (E) spectra acquired for **Cy5-NO₂** in different solvents. Optical spectra were recorded at 20 μM. For emission spectra that was excited at 500 nm.

Photophysical properties of Cy5-NO₂

The absorption and fluorescence spectra of the NTR probes were assessed in a PBS buffer (10 mM, pH 7.4) with 1% v/v DMSO at 37 °C. As shown in Fig. 1B and 1C, the probe **Cy5-NO₂** exhibited an intense absorption peak at 578 nm corresponding to the π-π* electronic transition, representing a significant blue shift of 220 nm relative to its precursor **Cy5-Cl**. Notably, this structural modification induced dramatic fluorescence quenching, as evidenced by the markedly diminished emission intensity compared to the unmodified precursor under identical experimental conditions. Furthermore, **Cy5-NO₂** demonstrated pronounced sensitivity to solvent polarity, as reflected by substantial spectral shifts observed during transitions from low-polarity to high-polarity solvents (Fig. 1D, 1E, and S2). In weakly



polar solvents such as dichloromethane (DCM), the probe displayed a pronounced bathochromic shift in its absorption spectrum ($\lambda_{\text{abs}} \approx 604$ nm) compared to polar solvents like water and dimethyl sulfoxide ($\lambda_{\text{abs}} \approx 578$ nm). The hypsochromic behavior observed across absorption, emission, and excitation profiles can be rationalized through solvation-induced stabilization mechanisms: polar solvents preferentially stabilize the polar ground-state (HOMO level) relative to the less polar first-excited state of the probe^{17,31,32}. This differential stabilization increases the HOMO–LUMO energy gap, thereby inducing the observed hypsochromic shifts in the electronic spectra. These solvent-dependent spectral variations underscore the probe's structural responsiveness to environmental polarity changes through solvatochromic

interactions. For potential applications in biological systems, the photostability of **Cy5-NO₂** was studied in phosphate buffered saline (PBS) solution under continuous white light irradiation for 40 minutes. No significant degradation of **Cy5-NO₂** was observed at its characteristic absorption wavelength (578 nm) (Fig. S3). This result underscores the remarkable photostability of **Cy5-NO₂** in PBS media. This contrasts sharply with conventional cyanine dyes, which typically degrade rapidly due to photoisomerization^{33,34} or aggregation^{35,36}. The enhanced stability arises from its rigid planar structure (as confirmed by X-ray crystallography) and the reduced number of inherent polyene linkers in the heptamethine structure³⁷.

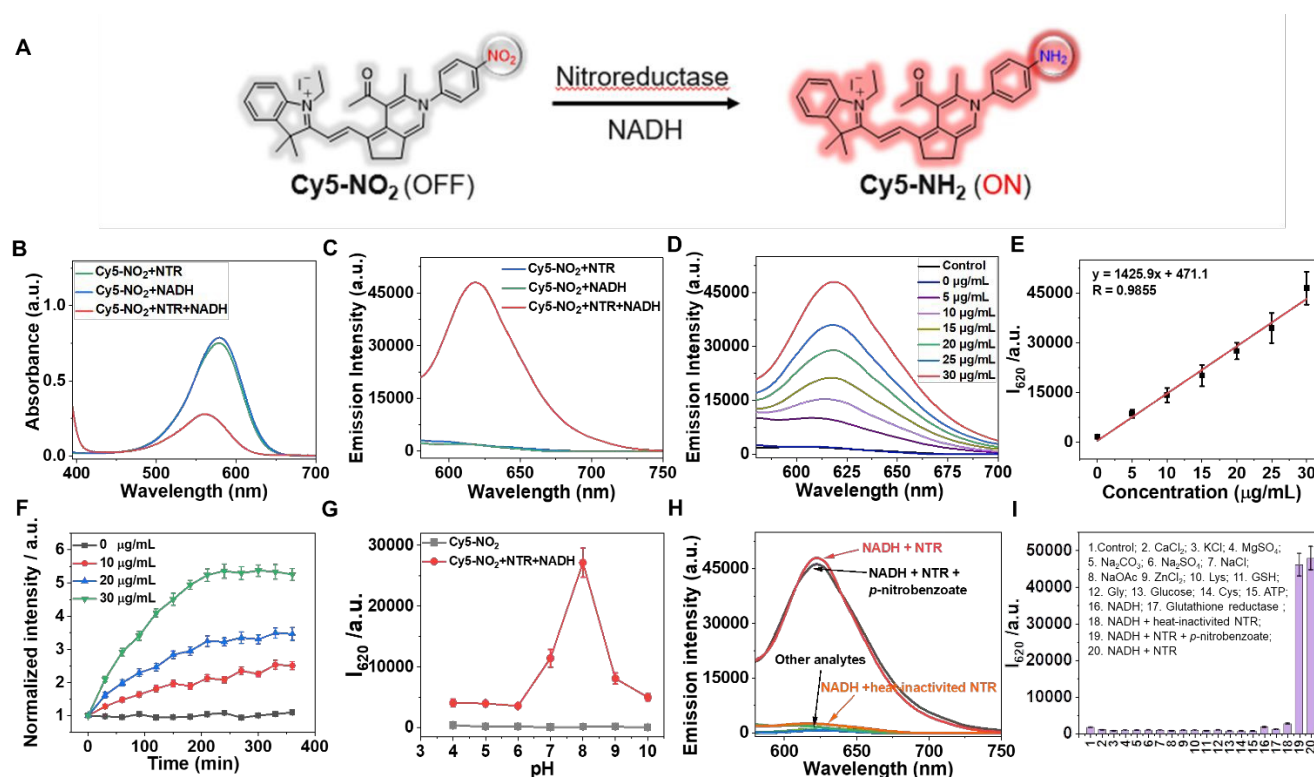


Fig. 2 (A) Proposed mechanism of **Cy5-NO₂**'s response to NTR activity. (B) Absorption and (C) emission spectra of **Cy5-NO₂** (20 μ M) in PBS buffer (10 mM, pH 7.4, with 10% DMSO), measured with or without NTR (20 μ g/mL) and/or NADH (500 μ M). (D) Sensitivity of the **Cy5-NO₂** probe (20 μ M) to varying concentrations of NTR (0–30 μ g/mL) in PBS buffer. (E) Linear correlation between fluorescence intensity at 620 nm (I_{620} nm) and NTR concentrations in the presence of NADH after a 60 min incubation at 37°C. (F) Normalized time-dependent fluorescence changes of **Cy5-NO₂** (20 μ M) in the presence of varying NTR concentrations (0, 10, 20, 30 μ g/mL). (G) Emission intensity of **Cy5-NO₂** probe (20 μ M) at 620 nm across different pH values in the presence of NTR (20 μ g/mL) and NADH (500 μ M) incubated in Britton-Robinson buffer solution at 37 °C for 60 min. (H and I) Emission intensity (I_{620} nm) of **Cy5-NO₂** (20 μ M) with different analytes (100 μ M each) after a 60 min incubation at 37°C in the presence of NTR (20 μ g/mL). Analytes include: 1. Blank, 2. CaCl₂, 3. KCl, 4. MgSO₄, 5. Na₂CO₃, 6. Na₂SO₄, 7. NaCl, 8. NaOAc, 9. ZnCl₂, 10. Lysine (Lys), 11. Glutathione (GSH), 12. Glycine (Gly), 13. Glucose, 14. Cysteine (Cys), 15. ATP, 16. NADH, 17. Glutathione reductase, 18. NADH + heat-inactivated NTR, 19. NADH + NTR + excess *p*-nitrobenzoate (a substrate analogue as competitor) and 20. NADH + NTR, $\lambda_{\text{ex}} = 500$ nm. Data represent mean values from three independent experiments. Error bars denote standard deviation (\pm SD).



Table 1 Fluorescence quantum yields of **Cy5-NO₂** in different solvent conditions in the absence and presence of NTR and NADH.

Φ_F	PBS (pH 7.4)	10% DMSO ^a	50% DMSO ^a	Pure DMSO	Pure EtOH	Pure THF	Pure DCM
Without NTR ^b	0.001	0.001	0.003	0.01	0.015	0.016	0.004
Φ_F	PBS (pH 7.4)	10% DMSO ^a	50% DMSO ^a	80% DMSO ^d	80% EtOH ^d	80% THF ^d	80% DCM ^d
With NTR ^{b,c}	0.022	0.093	0.068	0.03	0.028	0.026	0.009

^a All solvent volumes were adjusted to a same final volume using PBS. ^b The solutions containing **Cy5-NO₂** (20 μ M) were incubated at 37 °C for 60 min. ^c This condition was tested in the presence of NTR (20 μ M) and NADH (500 μ M). ^d The solution was prepared by 0.8 mL NTR (100 μ g/mL in water) with 3.2 mL pure organic solvent.

NTR response of **Cy5-NO₂** in aqueous

The NTR response properties of **Cy5-NO₂** were assessed in a PBS buffer solution (10 mM, pH 7.4, with 10% DMSO³⁸⁻⁴⁰), both in the presence and absence of NADH with a 60-minute incubation period. As shown in Fig. 2B, when either NADH (500 μ M) or NTR (20 μ g/mL) was individually added to the probe, no significant change was observed in the absorption peak of the reaction system, which remained centered around 578 nm. However, its absorption was blue-shift to 562 nm which triggered by the presence of both NTR and NADH. Additionally, under 500 nm excitation, no apparent change in fluorescence intensity upon individual addition of NADH or NTR. Consistent with the absorption spectra, a significant enhancement in fluorescence emission (approximately 30-fold) centered at 620 nm was observed when both NTR and NADH were added (Fig. 2C). This suggests that the observed fluorescence enhancement is attributable to the NTR-catalyzed reduction of the nitro group in the presence of NADH, yielding the reduced product **Cy5-NH₂** (Fig. 2A), a transformation corroborated by HR-ESI-MS analysis that detected the corresponding $[M + H]^+$ ion at m/z 464.2698 (Fig. S4). These results further confirm that the "turn-on" fluorescence of the probe is attributed to the catalytic reduction of the nitro group by NTRs.

To evaluate the sensitivity of the **Cy5-NO₂** probe toward NTR, fluorescence spectra were recorded at NTR concentrations from 0 to 30 μ g/mL (in 5 μ g/mL increments). As NTR concentration increased, the fluorescence intensity at 620 nm (I_{620} nm) gradually enhanced, peaking at 30 μ g/mL (Fig. 2D). The I_{620} nm against NTR concentration plot showed a strong linear relationship within 0–30 μ g/mL (Fig. 2E). Based on the formulae for limit of detection ($LOD = 3\sigma/k$) and limit of quantification ($LOQ = 10\sigma/k$), where σ represents the standard deviation of the blank signal and k is the slope of the calibration curve, the LOD and LOQ were determined to be 10 ng/mL and 33.3 ng/mL, respectively. These results demonstrate the probe's high sensitivity, enabling precise and quantitative detection of NTR at low concentrations.

Fluorescence Quantum yields measurements

Absolute fluorescence quantum yield measurements of **Cy5-NO₂** were conducted both in the absence and presence of NTR and NADH across seven solvent systems to evaluate the probe's behavior under varying conditions. In the absence of NTR and NADH, **Cy5-NO₂** exhibited strong fluorescence quenching ($\Phi_F <$

0.003) in aqueous or low-DMSO environments (<50%), primarily attributed to efficient intramolecular charge transfer (ICT), which dominates non-radiative decay pathways. Similarly, in low-polarity solvents such as DCM, the quantum yield remained low due to stabilization of the charge-transfer state, consistent with the observed red shift in the absorption spectrum compared to other solvents. In contrast, more polar organic solvents yielded Φ_F values between 0.01 and 0.016, indicating partial suppression of the ICT process.

In the presence of NTR and NADH, a significant increase in quantum yield was observed, confirming the enzymatic reduction of the nitro group and the subsequent "turn-on" fluorescence response of **Cy5-NH₂**. Among all tested conditions, the highest quantum yield ($\Phi_F = 0.093$) was achieved in PBS containing 10% DMSO. Increasing the DMSO concentration to 50% resulted in a ~27% decrease relative to the peak value, while at 80% DMSO, the quantum yield dropped by ~70%. A similar sharp decline was observed in other high-concentration organic solvent systems (e.g., 80% ethanol or 80% THF in PBS). This reduction is likely linked to structural disruption or denaturation of the enzyme, leading to markedly reduced catalytic activity. The relatively low quantum yield in pure PBS ($\Phi_F = 0.022$) may stem from poor probe solubility, which was significantly improved by the addition of 10% DMSO. These findings not only provide deeper insight into the photophysical behavior of **Cy5-NO₂** but also support its reliability and performance in complex biological environments.

Dynamic studies of **Cy5-NO₂**

To evaluate the kinetic properties of **Cy5-NO₂**, changes in fluorescence intensity at 620 nm (I_{620} nm) were monitored over time (0–360 min) at various NTR concentrations (0–30 μ g/mL) in the presence of NADH (Fig. 2F). Upon adding NTR, the fluorescence intensity at 620 nm increased gradually and stabilized by approximately 200 min, demonstrating the probe's reliability for NTR detection.

Effect of pH on **Cy5-NO₂**

The fluorescence response of a probe can be significantly influenced by pH levels. Therefore, an investigation was conducted to assess how pH variations impact the emission intensity at 620 nm of **Cy5-NO₂** (Fig. 2G). In the presence of NTR and NADH, **Cy5-NO₂** demonstrated significant fluorescence emission over a pH ranging from 6 to 10, with its efficiency peaking around pH 8.0. Considering



the practical application of the probe in biological systems, a pH of 7.4 was chosen for all subsequent experiments.

Selectivity

The selectivity of **Cy5-NO₂** for NTR was evaluated by comparing its response to various substances, including inorganic salts, amino acids, reductive agents, sugars, thiol-containing compounds, unrelated enzyme, substrate analogue for competing and heat-inactivated NTR. As demonstrated in Fig. 2H and 2I, **Cy5-NO₂** exhibited a pronounced fluorescence enhancement at 620 nm exclusively under the combined presence of NTR and NADH. Notably, co-incubation of the probe with NTR, NADH, and *p*-nitrobenzoate (a substrate analogue) at equimolar concentrations showed no significant difference in fluorescence intensity compared to the system without the analogue, confirming that the enzymatic catalysis of the probe remains unaffected by the presence of structurally related molecules. Furthermore, thermal inactivation of NTR through heating at 80 °C for 30 minutes completely abolished the fluorescence enhancement, confirming the enzymatic activity dependence of the response. Control experiments revealed negligible fluorescence changes in the presence of individual components (NTR or NADH) or other tested substances, underscoring the system's high selectivity. These findings collectively establish **Cy5-NO₂** as a highly specific fluorescent probe for NTR detection, with robust resistance to both competitive inhibition and non-specific interactions, thereby ensuring reliable and accurate enzymatic sensing.

Calculation study

To investigate the mechanism underlying the fluorescence changes of **Cy5-NO₂** and its product **Cy5-NH₂** upon reaction with NTR, we performed time-dependent density functional theory (TDDFT) calculations. As depicted in Fig. 3, in the excited state of **Cy5-NO₂**, the highest occupied molecular orbital (HOMO) is predominantly localized on the benzindole and the middle heterocyclic moiety, whereas the lowest unoccupied molecular orbital (LUMO) is only situated within the nitrobenzene unit. This spatial separation between the HOMO and LUMO results in significant charge transfer, which effectively quenches fluorescence. In contrast, after reduction by NTR, the transformation of **Cy5-NO₂** into **Cy5-NH₂** leads to a redistribution of the frontier orbitals. Both the HOMO and LUMO are confined to the benzindole and the middle heterocyclic region, corresponding to a local excitation (LE) state. This transition promotes substantial fluorescence emission. Consistent with this observation, the calculated oscillator strength (*f*) for **Cy5-NH₂** is 0.8750, markedly higher than that of **Cy5-NO₂** (0.0014), further corroborating the observed enhancement in fluorescence.

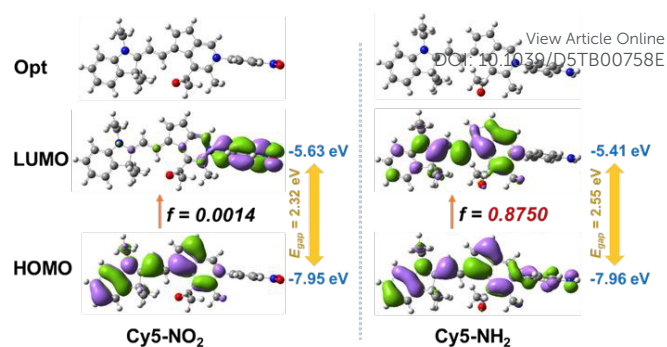


Fig. 3 The HOMO/LUMO frontier molecular orbitals and oscillator strength (*f*) calculated by TDDFT of **Cy5-NO₂** (left) and **Cy5-NH₂** (right) under the singlet excited states, respectively.

Inhibitory test of NTR activity

Dicoumarol(Dic), a competitive inhibitor of NADH, was employed to suppress NTR activity allowing the evaluation of the NTR probes' detection efficacy. Upon addition of 300 μM dicoumarol, a notable decrease in the fluorescence signal of the probe was observed (Fig. S5). This result verify that the fluorogenic response of the NTR probes is exclusively dependent on the presence of active NTR enzymes.

Bacterial detection by NTR probe

NTRs are universally present in bacteria. Due to the probe's strong responsiveness to NTR, making it suitable for fluorescence imaging as a "turn-on" probe, we propose its use for detecting bacterial nitroreductases produced during bacterial growth. *E. coli* and *S. aureus* were chosen as model pathogenic bacteria for the experiment. To determine the optimal concentration for bacterial detection, we evaluated the fluorescence behavior of the probe across a range of concentrations (Fig. 4A and 4B). The results demonstrated a concentration-dependent increase in fluorescence intensity, with *E. coli* exhibiting the most pronounced response. Considering both the need for sufficient signal strength and the desire to minimize probe usage, 20 μM was selected as the optimal concentration for subsequent experiments, as it provided robust fluorescence while avoiding excessive reagent consumption. Furthermore, to confirm the specificity of the probe toward nitroreductase (NTR) activity, we performed additional experiments using Dic. The emission intensity of the bacteria was measured after incubation with the probe, both in the presence and absence of Dic (Fig. 4C and 4D). The results revealed a significant increase in the fluorescence intensity of **Cy5-NO₂** following incubation with different bacterial strains, surpassing the control group. However, upon adding Dic to the bacterial solution, the fluorescence intensity decreased to the level of the control group, indicating that the fluorescence was directly linked to the enzymatic activity of NTRs in the bacteria. Taken together, these findings validate the probe's efficacy and specificity for nitroreductase detection in bacteria, and we propose that 20 μM can be the optimal concentration of **Cy5-NO₂** for bacterial imaging.



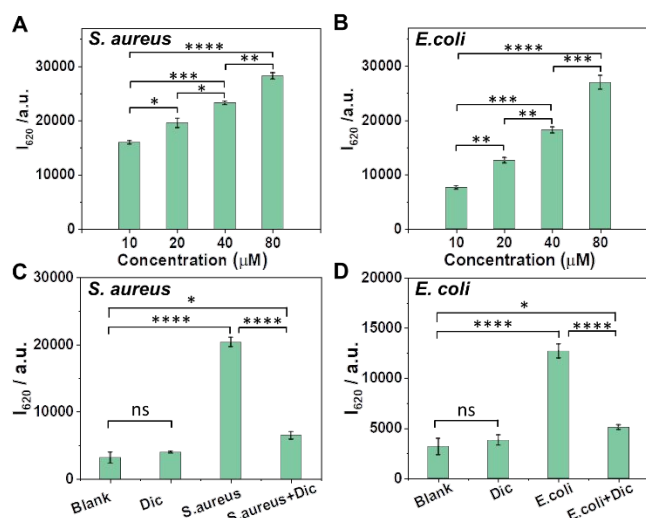


Fig. 4 Fluorescence detection of live bacteria using $Cy5-NO_2$. Fluorescence measurements were carried out after incubating (A) *S. aureus* and (B) *E. coli* with varying concentrations of $Cy5-NO_2$, or (C) *S. aureus* and (D) *E. coli* with 20 μM $Cy5-NO_2$ in the presence or absence of 0.1 mM Dic, for 60 min at 37°C. Fluorescence was measured at λ_{ex} = 500 nm and λ_{em} = 620 nm. This assay demonstrates the response of live bacterial cells to $Cy5-NO_2$ under different experimental conditions. Blank group means $Cy5-NO_2$ in PBS without bacteria. Error bars represent standard deviation (n = 3 independent replicates). Statistical significance was calculated via Student's t-test, **** p < 0.0001, * p < 0.05, p > 0.05 not considered statistically significant (ns).

Detection limits of the NTR probe

To determine the minimum detectable colony-forming unit (CFU) of $Cy5-NO_2$, its response was evaluated toward pathogenic *E. coli* (Gram-negative), *S. aureus* (Gram-positive), and methicillin-resistant *S. aureus* (MRSA). Bacterial cultures were incubated with $Cy5-NO_2$ (20 μM for 1 h), and fluorescence intensity at 620 nm was quantified. A dose-dependent increase in fluorescence was observed across all three bacterial strains as CFU concentrations increased (Figure S19). Notably, $Cy5-NO_2$ exhibited a significant fluorescence response at 3×10^6 CFU/mL for *E. coli* and *S. aureus*, whereas MRSA required a higher detection threshold of 5×10^6 CFU/mL. This sensitivity profile highlights the potential of $Cy5-NO_2$ as a diagnostic tool for bacterial infections, particularly in clinical settings where rapid identification of both Gram-negative and Gram-positive pathogens is crucial. The ability to detect MRSA at clinically relevant concentrations further underscores its applicability in monitoring antibiotic-resistant infections, which are associated with high morbidity and mortality in hospital settings. This discrepancy may be attributed to MRSA-specific features, such as enhanced cell wall rigidity or altered enzymatic activity, which could hinder the probe's interaction with the bacterial target⁴¹.

Bacterial imaging and visual detection by NTR probe

To visualize the detection of live bacterial cells with the probe, a confocal laser scanning microscope (CLSM) was utilized. Hoechst dye was utilized to stain live bacterial DNA, emitting blue fluorescence, while the probe generated red fluorescence through its interaction with bacterial NTRs. As illustrated in Fig. 5A and 5C, robust red fluorescence was observed for both *E. coli* and *S. aureus* bacterial strains. Notably, in the groups pre-incubated with Dic, the red fluorescence intensity was significantly quenched, confirming that the red fluorescence

was indeed due to the catalytic reduction of $Cy5-NO_2$ by bacterial NTRs (Fig. 5B and 5D). These findings highlight that $Cy5-NO_2$ holds great potential as a "turn-on" probe for detecting and imaging live bacterial cells with a strong fluorescence response.

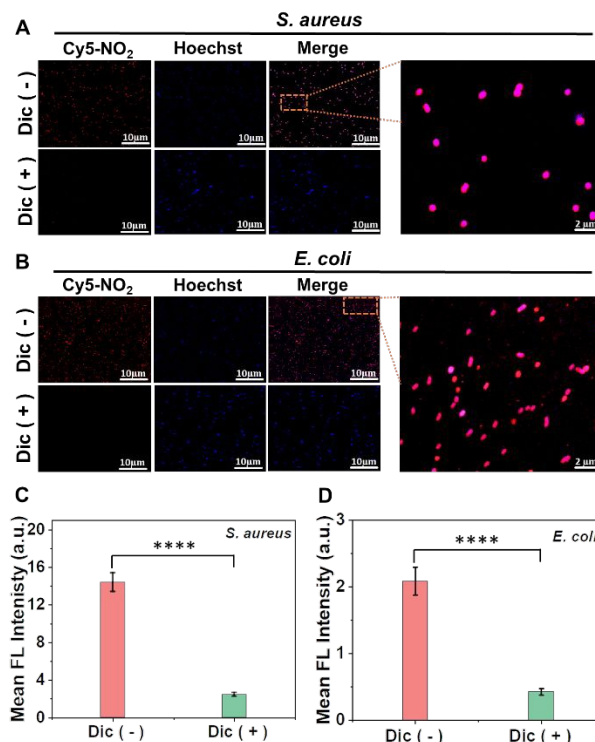


Fig. 5 Confocal laser scanning microscopy images of $Cy5-NO_2$ (20 μM) co-incubated with (A) *S. aureus* and (B) *E. coli*, both in the absence and presence of 0.1 mM Dic for 60 min at 37°C. Panels (C) and (D) display the corresponding mean fluorescence intensities of the red channel. Fluorescence intensity measurements of $Cy5-NO_2$ in bacterial cells. Imaging experiments were conducted using excitation/emission wavelength pairs of 405 nm/410–480 nm for Hoechst and 552 nm/600–650 nm for $Cy5-NO_2$. The laser power was set at 10% for Hoechst and 15% for $Cy5-NO_2$ to minimize photobleaching. Fluorescence intensities were quantified from the bacteria in the image by an ImageJ software. Error bars represent standard deviation (n = 3 independent replicates). Statistical significance was calculated via Student's t-test, **** p < 0.0001. Scale bar: 10 μm .

Conclusion

In summary, we have developed $Cy5-NO_2$, a highly sensitive and selective fluorescent probe for real-time monitoring of bacterial nitroreductase (NTR) activity. This probe operates via a streamlined mechanism of direct nitro-to-amine reduction, eliminating auxiliary functional groups that are prone to hydrolytic enzyme interference, such as esterases or proteases, which are common limitations in prior systems. The design of $Cy5-NO_2$ ensures exceptional stability, as evidenced by its resistance to degradation under continuous irradiation and its rigid planar structure confirmed by X-ray crystallography. Upon NTR-mediated reduction, the probe exhibits a dramatic 30-fold fluorescence enhancement at 620 nm, with a detection limit of 10 ng/mL, demonstrating improved performance in sensitivity and stability compared to most previously reported NTR-targeted probes. Time-dependent density functional theory



(TDDFT) calculations reveal that this "turn-on" mechanism arises from a transition from charge-transfer quenching in the nitro form (**Cy5-NO₂**) to local excitation in the reduced amine form (**Cy5-NH₂**), supported by a calculated oscillator strength increasing from 0.0014 to 0.8750. High-resolution mass spectrometry (HR-MS) analysis confirms the formation of **Cy5-NH₂** post-reduction, validating the theoretical predictions. The probe's high specificity for NTR under physiological conditions and its compatibility with standard confocal microscopy enable robust detection and imaging of live bacterial cells, such as *E. coli* and *S. aureus*, as demonstrated by confocal laser scanning microscopy (CLSM). Furthermore, its column-free synthesis (92 % yield) and minimal enzymatic interference position it as a scalable platform for industrial translation. These features collectively highlight **Cy5-NO₂** as a transformative tool for sensitive and specific bacterial detection, addressing critical gaps in current technologies and advancing applications in clinical diagnostics, microbial imaging, and targeted antimicrobial strategies.

Experimental

Materials and instruments

Unless otherwise stated, all solvents and reagents were commercially available and used without further purification. Escherichia coli nitroreductase (NTR) was obtained from Shanghai yuanye Bio-Technology Co., Ltd. The NTR was dissolved in ultrapure water (Milli-Q IQ 700), and the resulting enzyme solution was immediately stored at -22 °C to preserve enzyme activity. Additionally, NTR was dissolved in ultrapure water to prepare a stock solution of 100 µg/mL for subsequent use. β-Nicotinamide Adenine Dinucleotide (NAD) hydrogen salt (NADH) was also obtained from Shanghai yuanye Bio-Technology Co., Ltd. High-resolution mass spectra were acquired using a Q-Exactive Hybrid quadrupole-Orbitrap mass spectrometer. The ¹H NMR and ¹³C NMR spectra were recorded on a Bruker AVANCE III 400 MHz and a Bruker AVANCE 101 Digital NMR Spectrometer, respectively, using CD₃CN-*d*₃ as the solvent and tetramethylsilane (TMS) as the internal reference. UV-vis absorption spectra were recorded on a SuperMax 2800MF UV-vis spectrophotometer, and fluorescence spectra were measured on a FL970 Fluorescence spectrophotometer with a 1 cm standard quartz cell. Confocal microscopy images of *E. coli* and *S. aureus* were acquired by a Leica LAS X confocal microscope. All bacterial strains used in this study were purchased from ATCC.

Spectral Measurement

All spectral measurements were performed under standardized conditions. A stock solution of **Cy5-NO₂** (10.0 mM) was prepared in DMSO, and NADH (10.0 mM) was dissolved in ultrapure water. For the assay, NTR was dissolved in ultrapure water to the desired concentration. A working solution containing **Cy5-NO₂** (20 µM) and NADH (500 µM) was prepared in 10 mM PBS buffer (pH 7.4) with 10% DMSO. Varying concentrations of NTR (0–30 µg/mL) were added to the mixture, which was then incubated at 37 °C for 60 minutes. Spectra were recorded at an excitation wavelength of 500 nm after thorough mixing and incubation. All photophysical experiments were

conducted in triplicate using independent sample preparations. Data are expressed as mean ± standard deviation (SD).

Fluorescence Quantum yields measurements

The absolute fluorescence quantum yield (Φ_F) of **Cy5-NO₂** was measured using a Hamamatsu C11347 Absolute Photoluminescence Quantum Yield Measurement System under two experimental conditions: (1) in the absence of NTR and NADH, and (2) in the presence of NTR (20 µM) and NADH (500 µM). For the first condition, seven solvent systems containing 20 µM **Cy5-NO₂** were prepared, including PBS (pH 7.4), PBS with 10% or 50% DMSO, pure DMSO, pure ethanol, pure tetrahydrofuran (THF), and pure dichloromethane (DCM). For the second condition, the stock NTR solution (100 µg/mL in water) was pre-mixed with organic solvents to achieve final concentrations of 20 µM NTR, and seven solvent systems containing 20 µM **Cy5-NO₂** were prepared in a total volume of 4 mL as follows: PBS (3.2 mL PBS + 0.8 mL NTR + 1.42 mg NADH), 10% DMSO (2.8 mL PBS + 0.4 mL DMSO + 0.8 mL NTR + 1.42 mg NADH), 50% DMSO (1.2 mL PBS + 2.0 mL DMSO + 0.8 mL NTR + 1.42 mg NADH), 80% DMSO (3.2 mL DMSO + 0.8 mL NTR + 1.42 mg NADH), 80% ethanol (3.2 mL ethanol + 0.8 mL NTR + 1.42 mg NADH), 80% THF (3.2 mL THF + 0.8 mL NTR + 1.42 mg NADH), and 80% DCM (3.2 mL DCM + 0.8 mL NTR + 1.42 mg NADH). All samples were incubated at 37 °C for 60 minutes to ensure complete enzymatic reduction of **Cy5-NO₂** to **Cy5-NH₂** prior to quantum yield measurements.

Selectivity, pH influence and Dynamic study of Probe

To evaluate the specificity of the probe for NTR, it was incubated with various species (100 µM each: NaCl, KCl, ZnCl₂, Na₂CO₃, Na₂SO₄, NaOAc, CaCl₂, MgSO₄, cysteine, lysine, glycine, glutathione, glucose, ATP (Adenosine Triphosphate), NADH, glutathione reductase, NADH + heat-inactivated NTR (heat at 80 °C for 30 min), NADH + NTR + excess *p*-nitrobenzoate (a substrate analogue as competitor) and (NADH + NTR) in PBS/DMSO at 37 °C for 60 minutes. The influence of pH on probe responsiveness to NTR was studied by measuring photoluminescence at varying pH levels (4–10) using the probe (20 µM) with NTR (20 µg/mL) and NADH (500 µM) incubated in Britton-Robinson buffer solution at 37 °C for 60 min. Kinetic properties were examined by monitoring fluorescence intensity changes over time for **Cy5-NO₂** (20 µM) with varying NTR concentrations (0–30 µg/mL). All spectra were recorded at 500 nm excitation after mixing and incubation. The selectivity experiment was conducted in triplicate using independent sample preparations. Data are expressed as mean ± standard deviation (SD).

Sensing mechanism of Cy5-NO₂ with NTR

To further verify this reduction process, we performed high-resolution mass spectrometry on the reaction mixture after treatment with NTR/NADH. Specifically, **Cy5-NO₂** (20 µM), NADH (500 µM) and NTR (20 µg/mL) were incubated in PBS buffer (10 mM, pH 7.4) at 37 °C for 60 min. After completion of the reaction, the mixture was extracted with dichloromethane (3 × 20 mL), dried over anhydrous sodium sulfate, and concentrated under reduced pressure. The resulting residue was analyzed by HR-ESI-MS, which clearly showed a molecular ion ([M + H]⁺) peak at *m/z* 464.2698.



Bacteria detection and imaging

Bacterial suspensions of *Escherichia coli* (*E. coli*) and *Staphylococcus aureus* (*S. aureus*) were treated with **Cy5-NO₂** (20 μ M) for 60 min at 37°C, both with and without Dic (0.1 mM), an NTR inhibitor. After incubation, fluorescence was measured to assess probe activation. Bacterial cells were cultured, treated with probes (20 μ M) and Dic (0.1 μ M), and incubated for 60 min at 37°C. Cells were harvested by centrifugation, washed twice with Tris-HCl buffer (50 mM, pH 7.4), and resuspended in PBS at one-tenth the original volume. The bacteria were then stained with Hoechst (3 μ M) for 5 min, washed twice, and resuspended in PBS. A suspension of stained cells was placed on a confocal dish and immobilized with an agar block for imaging. Confocal microscopy images were obtained using a LAS X confocal microscope equipped with a 63 \times oil immersion objective lens. Two imaging channels were employed: Channel 1 (Hoechst 33342) was excited at 405 nm with emission detected between 410–480 nm (blue channel); Channel 2 (**Cy5-NO₂**) utilized an excitation wavelength of 552 nm and emission detection at 600–650 nm (red channel). Image acquisition was performed in 3D z-stack mode (5 slices, 0.5 μ m step size) with a pixel resolution of 1024 \times 1024. To minimize photobleaching, laser power was set to 10% for Hoechst 33342 and 15% for **Cy5-NO₂**. Hoechst 33342 was used to visualize bacterial DNA, while **Cy5-NO₂** was employed to monitor the fluorescent response of the probe. This protocol enabled clear and reliable analysis of bacterial samples. Post-acquisition image processing was conducted using LAS X v3.7 software.

Computational calculations

All the theoretical calculations are done by using based on the density functional theory (DFT) and time-dependent density functional theory (TD-DFT) based on B3LYP/6-31G(d,p) basis set which performed on Gaussian 09 software package.

Statistical analysis

All experiments were performed three times and the data were presented as means \pm standard deviation. Statistical analysis was performed according to the Student's t-test and one-way ANOVA analysis. Differences were considered statistically significant at the following p values: * $p < 0.05$, and **** $p < 0.0001$, $p > 0.05$ not considered statistically significant (ns).

Synthesis of Cy5-acac

Synthesis of Cy5-acac. A mixture of **Cy5-Cl** (1.0 g, 1.6 mmol), 2 mL acetylacetone and 8 mL triethylamine (Et₃N) were added into a round bottom flask with 40 mL DCM. The solution was refluxed for 4 h under N₂. Then removed the solvent and dissolved the solid in 30 mL MeOH with 1 mL saturated NH₄PF₆ aqueous solution for 1 h. The solvent was removed by vacuum rotary evaporation. The crude product was purified by silica gel using ethyl acetate: acetonitrile (50:1 to 10:1) as the eluent to obtain the pure product as green powder (0.8 g, 61.5%). ¹H NMR (500 MHz, CD₃CN-*d*₃) δ 7.55 – 7.46 (m, 4H), 7.43 (td, $J = 7.8, 1.1$ Hz, 2H), 7.26 (t, $J = 7.5$ Hz, 4H), 6.09 (d, $J = 14.0$ Hz, 2H), 4.12 (q, $J = 7.2$ Hz, 4H), 3.01 (s, 4H), 1.99 (s, 6H), 1.58 (s, 12H), 1.38 (t, $J = 7.2$ Hz, 6H). ¹³C NMR (101 MHz, CD₃CN-*d*₃) δ 191.55, 170.33, 143.38, 142.22, 141.26, 137.80, 128.65, 124.83, 122.34, 110.67, 104.81, 101.66, 48.97, 39.18, 27.36, 27.16, 22.52, 11.53. HRMS(ESI). Theoretical calc. C₃₈H₄₅O₂N₂PF₆ [M-PF₆]⁺ : $m/z = 561.34756$; found: [M-PF₆]⁺ $m/z = 561.34491$.

Synthesis of Cy5-NO₂

To 1.37 g (2 mmol) of **Cy5-acac** and 1.38 g (10 mmol) of p-nitroaniline in a 50 mL single-neck flask, 30 mL of toluene was added. The mixture was heated under reflux away from light for 12 hours. After the reaction was completed, a large amount of precipitate was formed. The mixture was filtered to retain the solid, yielding pure blue-violet solid **Cy5-NO₂**, 1.15 g, 92%. Blue crystals were obtained by diffusion system of acetonitrile and diethyl ether. ¹H NMR (500 MHz, CD₃CN-*d*₃) δ 8.51 – 8.47 (m, 2H), 7.88 (s, 1H), 7.79 – 7.76 (m, 2H), 7.48 – 7.42 (m, 2H), 7.36 (td, $J = 7.8, 1.2$ Hz, 1H), 7.14 (td, $J = 7.5, 0.8$ Hz, 1H), 7.09 (d, $J = 7.9$ Hz, 1H), 5.70 (d, $J = 12.7$ Hz, 1H), 3.97 (q, $J = 7.2$ Hz, 2H), 3.23 – 3.01 (m, 4H), 2.70 (s, 3H), 2.16 (s, 3H), 1.58 (s, 6H), 1.31 (t, $J = 7.1$ Hz, 3H). ¹³C NMR (126 MHz, CD₃CN-*d*₃) δ 203.89, 167.39, 153.38, 149.00, 146.09, 145.65, 142.68, 141.87, 140.28, 136.65, 128.98, 128.36, 128.32, 125.75, 125.59, 122.92, 122.05, 109.00, 96.49, 47.49, 37.83, 31.50, 28.47, 27.62, 26.11, 17.66, 10.78. HRMS (ESI). Theoretical calc. for C₃₁H₃₂N₃O₃ [M-I]⁺ : $m/z = 494.24382$; found: [M-I]⁺ $m/z = 494.24402$.

Synthesis of Cy5-NH₂

To 1.37 g (2 mmol) of **Cy5-acac** and 1.07 g (10 mmol) of p-nitroaniline in a 50 mL single-neck flask, 30 mL of toluene was added. The mixture was heated under reflux away from light for 12 hours. After the reaction was completed, a large amount of precipitate was formed. The mixture was filtered to retain the solid. Purification was carried out by silica gel column chromatography using dichloromethane as the eluent, yielding pure reddish-purple solid **Cy5-NH₂**, 0.88 g, 75.2%. ¹H NMR (500 MHz, CD₃CN-*d*₃) δ 7.93 (s, 1H), 7.40 – 7.30 (m, 3H), 7.18 – 7.12 (m, 2H), 7.09 (td, $J = 7.5, 0.7$ Hz, 1H), 7.02 (d, $J = 7.9$ Hz, 1H), 6.90 – 6.73 (m, 2H), 5.63 (d, $J = 12.7$ Hz, 1H), 3.92 (q, $J = 7.2$ Hz, 2H), 3.29 – 2.98 (m, 4H), 2.68 (s, 3H), 2.19 (s, 3H), 1.57 (s, 6H), 1.27 (t, $J = 7.3$ Hz, 3H). ¹³C NMR (126 MHz, CD₃CN-*d*₃) δ 203.98, 165.89, 152.87, 150.11, 147.27, 142.92, 141.89, 140.02, 138.49, 134.89, 130.57, 129.48, 128.25, 126.77, 126.02, 122.37, 121.98, 114.46, 108.52, 95.56, 46.92, 37.53, 31.41, 28.35, 27.66, 26.19, 17.47, 10.63, 8.18. HRMS (ESI). Theoretical calc. for C₃₁H₃₄N₃O [M-I]⁺ : $m/z = 464.26964$; found: [M-I]⁺ $m/z = 464.26965$.

X-ray crystallography

Single crystal of **Cy5-NO₂** suitable for X-ray diffraction studies were grown by slow vapor diffusion of diethyl ether into acetonitrile solution. Single-crystal X-ray diffraction analysis were performed on a Bruker APEX-II CCD diffractometer with graphite-monochromated Mo K_{α} radiation ($\lambda = 0.71073$ Å) at 293 K, 150 K, 170 K. All absorption corrections were performed using multiscan. The structure was solved by direct methods and refined by full-matrix least-squares techniques on F^2 with the SHELXL-97 or SHELXL-2014 program package. CCDC-2423384 contain the supplementary crystallographic data of **Cy5-NO₂**. This data can be obtained free of charge from The Cambridge Crystallographic Data Centre via www.ccdc.cam.ac.uk/data_request/cif.

Author contributions

Jiqiang Liu: Conceptualization, Data curation, Investigation, Methodology, Validation, Writing-original draft, Writing-review & editing. Abdulkadir Zakari Abdulkadir: Data curation, Investigation, Methodology, Validation. Siye Wu: Data curation, Investigation. Yonghui Gao: Investigation, Validation. Baraka Joseph Butuyuyu: Investigation, Validation. Keith Man-Chung Wong: Resources,



Writing-review & editing. Chi-Sing Lee: Resources, Writing-review & editing. Lintao Cai: Writing-review & editing. Jihong Chen: Funding acquisition, Resources. Pengfei Zhang: Conceptualization, Funding acquisition, Resources, Supervision, Writing-review & editing.

Conflicts of interest

There are no conflicts to declare.

Data availability

The data supporting this article have been included as part of the Supplementary Information.

Acknowledgements

We are grateful for the financial support from National Key R&D Programs (China) (2021YFA0910001), the National Natural Science Foundation of China (82470719, 22105057, 81901906, 32000982), Guangdong Provincial Key Area R&D Program (2020B1111540001), Guangdong Province Basic and Applied Basic Research Fund Enterprise Joint Fund (2023A1515220119), the Shenzhen Science and Technology Program (KQTD20210811090115019), Shenzhen Basic Research (key project) (China) (JCYJ20210324120011030, JCYJ20210324115804013, and JCYJ20200109114616534), the Major Instrumentation Development Program of the Chinese Academy of Sciences (Project Number: ZDKYYQ20220008), Guangdong Basic and Applied Basic Research Fund Project (China) (2019A1515110222 and 2021A1515110699). The acknowledgements come at the end of an article after the conclusions and before the notes and references.

References

- 1 S. Altveş, H. K. Yildiz and H. C. Vural, *Biosci. Microbiota, Food Heal.*, 2020, **39**, 23.
- 2 M. Kamel, S. Aleya, M. Alsubih and L. Aleya, *J. Pers. Med.*, 2024, **14**, 217.
- 3 A. El-Sayed, L. Aleya and M. Kamel, *Environ. Sci. Pollut. Res.*, 2021, **28**, 28926.
- 4 A. El-Sayed, L. Aleya and M. Kamel, *Environ. Sci. Pollut. Res.*, 2021, **28**, 36967.
- 5 A.-P. Baciú, C. Baciú, G. Baciú and G. Gurau, *J. Med. Life*, 2024, **17**, 246.
- 6 F. M. E. Wagenlehner and F. Dittmar, *Eur. Urol.*, 2022, **82**, 658.
- 7 K. S. Ikuta, L. R. Swetschinski, G. R. Aguilar, F. Sharara, T. Mestrovic, A. P. Gray, et al., *Lancet*, 2022, **400**, 2221.
- 8 A. Elbehiry, E. Marzouk, A. Abalkhail, M. H. Abdelsalam, M. E. A. Mostafa, M. Alasiri, M. Ibrahim, A. T. Ellethy, A. Almuzaini, S. N. Aljarallah, A. Abu-Okail, N. Marzook, S. Alhadyan and H. M. Edrees, *Front. Microbiol.*, 2025, **16**, 1.
- 9 E. Sauerborn, N. C. Corredor, T. Reska, A. Perlas, S. Vargas da Fonseca Atum, N. Goldman, N. Wantia, C. Prazeres da Costa, E. Foster-Nyarko and L. Urban, *Nat. Commun.*, 2024, **15**, 1.
- 10 M. A. Salam, M. Y. Al-Amin, J. S. Pawar, N. Akhter and I. B. Lucy, *Saudi J. Biol. Sci.*, 2023, **30**, 103582.
- 11 B. Zhang, H. Chen, L. Shi, R. Guo, Y. Wang, Y. Zheng, R. Bai, Y. Gao, B. Liu and X. Zhang, *ACS Sensors*, 2024, **9**, 4560.
- 12 S. Lepuschitz, T. Weinmaier, K. Mrazek, S. Beisken, J. Weinberger and A. E. Posch, *Front. Microbiol.*, 2020, **11**, 1883.
- 13 S. Y. Park, S. A. Yoon, Y. Cha and M. H. Lee, *Coord. Chem. Rev.*, 2021, **428**, 213613.
- 14 M. H. Lee, J. S. Kim and J. L. Sessler, *Chem. Soc. Rev.*, 2015, **44**, 4185.
- 15 S. A. Yoon, S. Y. Park, Y. Cha, L. Gopala and M. H. Lee, *Front. Chem.*, 2021, **9**, 1.
- 16 Y. Yao, J. Ma, S. Xing, F. Zeng, L. Wu, Y. Li, J. Du, Q. Yang and Y. Li, *Anal. Chim. Acta*, 2024, **1292**, 342259.
- 17 N. I. Wickramasinghe, B. Corbin, D. Y. Kanakarathna, Y. Pang, C. S. Abeywickrama and K. J. Wijesinghe, *Biosensors*, 2023, **13**, 799.
- 18 B. Zhu, X. Xing, J. Kim, H. Rha, C. Liu, Q. Zhang, L. Zeng, M. Lan and J. S. Kim, *Biomaterials*, 2024, **304**, 122419.
- 19 A. Mukherjee and S. E. Rokita, *J. Am. Chem. Soc.*, 2015, **137**, 15342.
- 20 M. D. Roldán, E. Pérez-Reinado, F. Castillo and C. Moreno-Vivián, *FEMS Microbiol. Rev.*, 2008, **32**, 474.
- 21 J. Zhang, M. Zhou, X. Li, Y. Fan, J. Li, K. Lu, H. Wen and J. Ren, *Talanta*, 2023, **254**, 124133.
- 22 J. Hira, M. J. Uddin, M. M. Haugland and C. S. Lentz, *Molecules*, 2020, **25**, 4949.
- 23 W. Gao, A. Shi, Y. Hou, P. Zhang, Q. Zhang and C. Ding, *Talanta*, 2025, **290**, 127804.
- 24 Z. Mi, L. Liu, Y. Zhao and J. Guan, *Int. J. Biol. Macromol.*, 2020, **164**, 932.
- 25 N. Plumeré, *Anal. Bioanal. Chem.*, 2013, **405**, 3731.
- 26 D. Yang, H. Y. Tian, T. N. Zang, M. Li, Y. Zhou and J. F. Zhang, *Sci. Rep.*, 2017, **7**, 2.
- 27 C. Zhang, K. Yan, C. Fu, H. Peng, C. J. Hawker and A. K. Whittaker, *Chem. Rev.*, 2022, **122**, 167.
- 28 J. J. Morsby, K. M. Atkinson, S. Shradha Reddy Kommidi, T. Freel, H. Janeková, P. Štacko and B. D. Smith, *Eur. J. Org. Chem.*, 2022, **2022**, e202200270.
- 29 S. Nisar and B. Sui, *Sens. Diagn.*, 2024, **3**, 1505.
- 30 A. F. Bedernjak, P. W. Groundwater, M. Gray, A. L. James, S. Orega, J. D. Perry and R. J. Anderson, *Tetrahedron*, 2013, **69**, 8456.
- 31 K. A. Bertman, C. S. Abeywickrama and Y. Pang, *ChemBioChem*, 2022, **23**, e202100516.
- 32 S. Cha, M. G. Choi, H. R. Jeon and S.-K. Chang, *Sensors Actuat. B-Chem.*, 2011, **157**, 14.
- 33 K. Jia, Y. Wan, A. Xia, S. Li, F. Gong and G. Yang, *J. Phys. Chem. A*, 2007, **111**, 1593.
- 34 J. Kabatc and J. Pączkowski, *Dyes and Pigments*, 2004, **61**, 1.
- 35 F. Bertocchi, A. Delledonne, G. Vargas-Nadal, F. Terenziani, A. Painelli and C. Sissa, *J. Phys. Chem. C*, 2023, **127**, 10185.
- 36 G. B. Behera, P. K. Behera and B. K. Mishra, *J. Surface Sci. Technol.*, 2007, **23**, 1.
- 37 R. R. Nani, J. A. Kelley, J. Ivanic and M. J. Schnermann, *Chem. Sci.*, 2015, **6**, 6556.
- 38 S. C. Cosgrove, G. J. Miller, A. Bornadel and B. Dominguez, *ACS Sustainable Chem. Eng.*, 2023, **11**, 8556.
- 39 S. Jiao, S. Yang, X. Meng and C. Wang, *Spectrochim. Acta A*, 2020, **241**, 118637.
- 40 H. Wang, M. Yang, M. Ji and P. Wang, *J. Photoch. Photobiol. A*, 2022, **427**, 113814.
- 41 N. A. Turner, B. K. Sharma-Kuinkel, S. A. Maskarinec, E. M. Eichenberger, P. P. Shah, M. Carugati, T. L. Holland and V. G. Fowler, *Nat Rev Microbiol*, 2019, **17**, 203.



Data availability statements

View Article Online
DOI: 10.1039/D5TB00758E

The data supporting this article have been included as part of the Supplementary Information.

